Published in final edited form as:
J Invest Dermatol. 2009 March ; 129(3): 573–583. doi:10.1038/jid.2008.276.

Endogenous Galectin-3 Is Localized in Membrane Lipid Rafts and Regulates Migration of Dendritic Cells

Daniel K. Hsu[1], **Alexander I. Chernyavsky**[2], **Huan-Yuan Chen**[1], **Lan Yu**[1], **Sergei A. Grando**[2], and **Fu-Tong Liu**[1]

1*Department of Dermatology, University of California Davis School of Medicine, Sacramento, California, USA*

2*Department of Dermatology, University of California Irvine School of Medicine, Irvine, California, USA*

Abstract

This study reveals a function of endogenous galectin-3, an animal lectin recognizing β-galactosides, in regulating dendritic cell motility both *in vitro*and *in vivo*,which to our knowledge is unreported. First, galectin-3-deficient ($gal3^{-/-}$) bone marrow-derived dendritic cells exhibited defective chemotaxis compared to $gal3^{+/+}$ cells. Second, cutaneous dendritic cells in $gal3^{-/-}$ mice displayed reduced migration to draining lymph nodes upon hapten stimulation compared to $gal3^{+/+}$ mice. Moreover, $gal3^{-/-}$ mice were impaired in the development of contact hypersensitivity relative to $gal3^{+/+}$ mice in response to a hapten, a process in which dendritic cell trafficking to lymph nodes is critical. In addition, defective signaling was detected in $gal3^{-/-}$ cells upon chemokine receptor activation. By immunofluorescence microscopy, we observed that galectin-3 is localized in membrane ruffles and lamellipodia in stimulated dendritic cells and macrophages. Furthermore, galectin-3 was enriched in lipid raft domains under these conditions. Finally, we determined that ruffles on $gal3^{-/-}$ cells contained structures with lower complexity compared to $gal3^{+/+}$ cells. In view of the participation of membrane ruffles in signal transduction and cell motility, we conclude that galectin-3 regulates cell migration by functioning at these structures.

INTRODUCTION

Inflammation is an important process of the immune system characterized by infiltration of leukocytes into tissue spaces (Thomas *et al.*, 1999; Germain, 2004; Ma and Pope, 2005). The initial stages of an innate immune response occur within hours of a stimulus and consist of infiltration of neutrophils, closely followed by monocytes and macrophages, spanning a few days, and then by lymphocytes (Schluger and Rom, 1997; Janeway and Medzhitov, 2002).

Monocytes and macrophages are important in inflammation, sharing early phagocytic functions with neutrophils to clear invading organisms or dead tissue and also secreting factors that recruit and activate other immune cells (Hume, 2006). Monocytes are capable of differentiating into dendritic cells (DCs), thus serving as a source of progenitor cells migrating into tissues (Sallusto and Lanzavecchia, 1994; Piemonti *et al.*, 1995; Palucka *et al.*, 1998). Impediments in monocyte trafficking will influence immune responses, as DCs operate as professional antigen-presenting cells and are crucial components of the immune system,

Correspondence: Dr Daniel K. Hsu, Department of Dermatology, University of California Davis School of Medicine, 4645 2nd Avenue, Room 3100, Sacramento, California 95817, USA. E-mail: dkhsu@ucdavis.edu.

CONFLICT OF INTEREST
The authors declare no conflicts of interest.

serving as a required bridge between innate and adaptive immunity. DC migration to lymph nodes upon induction with antigen is critical during initial stages of antigen-specific immune responses (Banchereau *et al.*, 2000).

DCs and macrophages express several proteins during activation and maturation; among these is galectin-3, a lectin recognizing β-galactosides (Liu, 2005). Galectin-3 is a pleiotropic protein with both intracellular and extracellular functions. In the intracellular domain, this protein has a number of different functions, including regulation of apoptosis, whereas in the extracellular domain, it activates cells and mediates cell aggregation and adhesion to the substratum (reviewed by Liu (2005), Nakahara *et al.* (2005), and Hughes (2001)).

To assist in elucidating the functions of galectin-3, we have generated a galectin-3 null ($gal3^{-/-}$) mouse strain. In earlier studies of these animals, we observed increased propensity for cell death in $gal3^{-/-}$ macrophages relative to $gal3^{+/+}$ cells upon activation. We also documented reduced levels of peritonitis in $gal3^{-/-}$ mice, compared to $gal3^{+/+}$ animals (Hsu *et al.*, 2000). More recently, we demonstrated defective macrophage phagocytosis in $gal3^{-/-}$ mice (Sano *et al.*, 2003). In the present study, we found that $gal3^{-/-}$ DCs exhibit impaired cell migration in responses to chemokines *in vitro* and to stimuli in the skin *in vivo*. As DC trafficking to lymph nodes is a critical process in antigen-specific inflammation responses, such as contact hypersensitivity (Larsen *et al.*, 1990; Forster *et al.*, 1999), we detected attenuated contact hypersensitivity responses in $gal3^{-/-}$ compared to $gal3^{+/+}$ mice. Additional studies revealed that galectin-3 partitions into membrane lipid rafts and galectin-3 deficiency results in structural differences in membrane ruffles, suggesting that deficiency of this protein in membrane microdomains may be responsible for impaired DC migration.

RESULTS

Galectin-3 is expressed in bone marrow-derived dendritic cells

Bone marrow cells cultured in the presence of recombinant mouse GM-CSF (rGM-CSF) were stained for galectin-3 with antibody and analyzed by flow cytometry. There was a gradual decrease in the amounts of intracellular galectin-3 during culture of immature dendritic cells (BMiDCs), as evaluated by flow cytometry, but barely detectable galectin-3 on cell surfaces (Figure 1a, bi). Levels of galectin-3 increased in DCs driven to maturation by lipopolysaccharide (LPS), and this was confirmed by immunoblotting analysis (Figure 1a inset, bi). In BMDCs matured with LPS, expression levels and composition of $gal3^{+/+}$ and $gal3^{-/-}$ populations were comparable (Figure 1bii, iii). In adherent BMiDCs, galectin-3 was detected by indirect immunofluorescence microscopy in the cytoplasm, cell membrane, and other subcellular regions (Figure 1c), but was undetectable in cells if not permeabilized with detergent (not shown). The specificity of the anti-galectin-3 antibody was demonstrated by very low background staining of similarly processed $gal3^{-/-}$ BMiDCs (Figure 1c).

In vitro migration of immature bone marrow-derived dendritic cells from $gal3^{-/-}$ mice is impaired

In a standard chemotactic assay, we observed significantly reduced migration of BMiDCs from $gal3^{-/-}$ mice to macrophage chemotactic protein-1 (MCP-1/CCL2) and macrophage inflammatory protein-1α (MIP1α/CCL3; Figure 2a and b) and macrophage colony-stimulating factor-1 (not shown). The influence of galectin-3 on DC migration appeared to be through intracellular action, because chemotaxis was unaffected by the presence of 20m_M lactose, an inhibitor of galectin-3 lectin activity, or 20m_M sucrose, a control sugar (data not shown). However, migration of $gal3^{-/-}$ BMDCs was unimpaired when matured for 24 hours in the presence of 2 mg ml^{-1} LPS (Figure 2c).

In parallel experiments, bone marrow-derived macrophages (BMMΦs) from gal3$^{-/-}$ mice demonstrated impaired chemotaxis to MCP-1/CCL2 and MIP1α/CCL3 compared to gal3$^{+/+}$ BMMΦs (not shown). As BMMΦs are adherent, we employed a nonchemotactic agarose invasion assay, in which cells were allowed to migrate spontaneously and randomly below a layer of agarose under normal culture conditions. BMMΦs from gal3$^{-/-}$ animals demonstrated impaired migration, as shown in Figure 2d. Under these culture conditions, no differences were observed in Annexin V binding to gal3$^{+/+}$ and gal3$^{-/-}$ macrophages, thus excluding the contribution of apoptosis in the observed differences.

In vivo migration of dendritic cells is impaired in gal3$^{-/-}$ mice

We then investigated *in vivo* cell migration by using BMiDCs labeled with the fluorescent vital dye $DiOC_{16}$. Labeled cells were injected into footpads of gal3$^{+/+}$ and gal3$^{-/-}$ mice and the labeled cells in draining lymph nodes were counted 2 days later. Lower numbers of gal3$^{-/-}$ than of gal3$^{+/+}$ BMDCs were detected in gal3$^{+/+}$ animals, although the difference was not statistically significant. In gal3$^{-/-}$ recipients, the migration of gal3$^{-/-}$ BMDCs was significantly lower than that of gal3$^{+/+}$ cells (Figure 3a), suggesting that defective migration of gal3$^{-/-}$ cells occurs *in vivo*.

We subsequently measured *in vivo* migration of endogenous cutaneous DCs in a model in which DCs migrate to draining lymph nodes in response to stimulus by a hapten, fluorescein isothiocyanate, which is taken up by DCs. We noted significantly lower numbers of fluorescein-labeled DCs in the lymph nodes of gal3$^{-/-}$ mice compared to gal3$^{+/+}$ mice at the 6 hour time point, but this defect was overcome after 24 hours (Figure 3b). We also examined epidermal sheets from these animals. The morphologies and densities of epidermal gal3$^{-/-}$ and gal3$^{+/+}$ DCs were indistinguishable (Figure 3c) and comparable between the two genotypes (Figure 3d). Thus, the above results are not due to lower densities of cutaneous DCs in gal3$^{-/-}$ mice.

Gal3$^{-/-}$ mice exhibit attenuated responses in a model of contact hypersensitivity

To evaluate if the defect observed in gal3$^{-/-}$ DC motility results in an *in vivo* phenotype, we employed an inflammatory model with the hapten oxazalone. As shown in Figure 4a, ear swelling in gal3$^{-/-}$ mice was significantly lower than in gal3$^{+/+}$ mice and this difference was maintained over the entire period of the assay. We also compared uptake and processing of antigen by BMiDCs from gal3$^{-/-}$ and gal3$^{+/+}$ mice, employing DQ-OVA, a poorly fluorescent ovalbumin derivative that is converted to highly fluorescent degradation products upon intracellular proteolytic processing. Figure 4b shows that gal3$^{-/-}$ and gal3$^{+/+}$ DCs exhibited parallel increases in enhanced fluorescence, and the difference between genotypes was not statistically significant, suggesting the absence of impaired antigen uptake and processing in gal3$^{-/-}$ cells. Furthermore, fluorescence intensity distributions were detected in virtually the same percentage of cells from both genotypes (data not shown).

Lymph node cell numbers and composition were similar by flow cytometry in gal3$^{+/+}$ and gal3$^{-/-}$ mice (Consortium for Functional Glycomics public data, 2008). Thorough histological analyses by immunofluorescence staining with antibody to major histocompatibility class II antigen confirmed similar densities and distribution of DCs in the paracortical regions of the lymph nodes, and histological staining detected no architectural deviations in gal3$^{-/-}$ versus gal3$^{+/+}$ lymph nodes (data not shown and Hsu *et al.*, 2000). These results suggest that the impaired hapten-specific inflammatory response to oxazalone observed in gal3$^{-/-}$ mice was not due to defects in lymph node structure or uptake and processing of antigen.

Immature gal3$^{-/-}$ DCs exhibit signaling defects in response to chemokine

To determine which defects in BMiDCs from gal3$^{-/-}$ mice contribute to impaired migration, we analyzed for phospho-AKT/PKB, a downstream target of PI3K activated by ligation of chemokine and cytokine receptors (Curnock *et al.*, 2002; Hawkins *et al.*, 2006). We observed significantly decreased levels of phospho-AKT in cells from gal3$^{-/-}$ mice compared to those from gal3$^{+/+}$ mice (Figure 5). Levels of pMAPK 1/2 in gal3$^{-/-}$ cells were also significantly lower than in gal3$^{+/+}$ BMiDCs. However, levels of phospho-MKK4, which signals through an alternate pathway (Curnock *et al.*, 2002), were unaffected in gal3$^{-/-}$ cells (data not shown).

Galectin-3 is localized in membrane ruffles of immature bone marrow-derived dendritic cells

In quiescent cells, galectin-3 was diffusely present in the cytosol, but the protein was concentrated in membrane ruffles (arrowheads, green in Figure 6a) in DCs exposed to chemokines. These staining patterns are intracellular, as galectin-3 is undetectable in nonpermeabilized cells. Galectin-3 was also concentrated in other regions of the membrane involved in locomotion, such as lamellipodia (arrows, Figure 6a) and the leading edge of polarized cells. These membrane structures are enriched in F-actin (Ridley *et al.*, 2003), as visualized by staining with labeled phalloidin (red in Figure 6a). By employing algorithms for co-localization analyses, we demonstrated co-dependent staining for galectin-3 and F-actin by diagonal distribution of pixels along the intensity dot plot of galectin-3 (green) versus F-actin (red) from all the DCs (Figure 6b).

Intensity correlation analysis (ICA) is another important objective measure of co-dependent staining between a pair of fluorescence channels and involves computation of intensity changes of corresponding pixels in each channel in relationship to normalized intensities. Output values are expressed as product difference of the means (PDM; Costes *et al.*, 2004; Li *et al.*, 2004). By this measure, co-localization of galectin-3 with F-actin is evident, because co-dependent pixel intensity variations, which appear as predominant positive skewing of PDM values, were observed for both proteins (Figure 6c). As shown in Figure 6d, regions of DCs that demonstrate high PDM values correspond to cell membranes that contain ruffles. The demonstration by ICA that microscopic co-staining of galectin-3 and F-actin varies in synchrony strongly indicates that the two proteins are co-localized.

An additional measure of co-dependence was obtained by evaluating Pearson's correlation coefficient (Manders *et al.*, 1993) for galectin-3 and F-actin staining. A large coefficient of 0.89 indicates a highly significant correlation between galectin-3 and F-actin pixel intensity profiles. This is further supported by large Manders' coefficients of 0.95 and 0.96 for M1 and M2, respectively (Manders *et al.*, 1993), which are consistent with the co-localization of galectin-3 with F-actin and F-actin with galectin-3, respectively. The above analytical procedures avoid cursory assignment of galectin-3 and F-actin co-localization merely by inspection.

Microscopic detection of galectin-3 in membrane lipid rafts of immature bone marrow-derived dendritic cells

Many cell surface receptors of growth factors and cytokines are associated with membrane lipid rafts, which are discrete domains containing high levels of cholesterol, sphingomyelin, and gangliosides (Brown and Rose, 1992; Parton and Simons, 1995). Membrane regions enriched in lipid rafts can be visualized with the aid of cholera toxin subunit B (CTB), which recognizes the raft ganglioside component GM1 (King and Van Heyningen, 1973; Spangler, 1992). We detected the presence of galectin-3 in membrane regions that were also stained with CTB on wild-type BMiDCs migrating on fibronectin (Figure 7a). As in Figure 6, membrane galectin-3 is located intracellularly and is detected only after permeabilization.

To objectively demonstrate co-localization of galectin-3 and CTB, we performed ICA as described above. Co-dependent changes in staining intensities of galectin-3 (green) and CTB (red) are evident from diagonal distribution of the fluorescence pixel intensities (Figure 7b) and further supported by distinctive positive skewing of PDM values (Figure 7c) for galectin-3 (green) and CTB (red). Co-localization of galectin-3 with CTB in membrane structures is also indicated by positive PDM values (Figure 7d). A large Pearson's correlation coefficient of 0.93, suggesting significant co-dependent staining of galectin-3 and CTB, is consistent with large Manders' coefficients of 0.97 and 0.95 for M1 and M2, respectively.

Galectin-3 is present in lipid rafts

We next sought biochemical evidence for localization of galectin-3 in membrane lipid rafts by using the mouse macrophage cell line J774A.1. The rafts were isolated in the presence of Na_2CO_3 (pH 11), highly stringent conditions that limit nonspecific association of proteins (Smart *et al.*, 1995). Immunoblotting analysis demonstrated that galectin-3 was present in low-density fractions containing lipid rafts (Figure 7e) that are stained positively for flotillin-1, a marker for lipid rafts (Bickel *et al.*, 1997; Figure 7e). To exclude the possibility that galectin-3 was present in the raft-enriched fractions, not as an intrinsic raft protein but bound to raft-associated glycoproteins through lectin interaction, we performed a similar isolation in sucrose gradients with the inclusion of 100m$_M$ lactose throughout the gradient as an inhibitor of galectin-3's lectin activity. Figure 7e shows that galectin-3 is still present in fractions containing lipid rafts, suggesting that this protein exists as a raft protein independent of its lectin activity.

Structural differences in ruffles of gal3$^{-/-}$ and gal3$^{+/+}$ cells

Cell migration induced by extracellular stimuli involves rapid membrane reorganization (Gungabissoon and Bamburg, 2003; Ridley *et al.*, 2003). In migrating cells, ruffles are rapidly formed over cell surfaces and reorganize to form cell structures that are associated with migration, such as pseudopods (Zigmond and Sullivan, 1979; Ridley *et al.*, 2003; Borm *et al.*, 2005). We thus employed quantitative methods to compare ruffle properties between gal3$^{+/+}$ and gal3$^{-/-}$ BMiDCs by using a semiautomated process that provides shape descriptors representing their physical characteristics (Yi and Coppolino, 2006). Surface ruffles were identified by their characteristic morphology in cells stained with labeled phalloidin and imaged by deconvolution fluorescence microscopy (Figure 8a). There were higher proportions of smaller ruffles and correspondingly lower proportions of larger structures in gal3$^{-/-}$ cells compared to gal3$^{+/+}$ cells, as measured by ruffle area and a related property, perimeter (Figure 8bi). In addition, ruffles on gal3$^{-/-}$ cells consisted of proportionately higher curl values than gal3$^{+/+}$ cells (Figure 8Bii). This indicates a lower degrees of ruffle convolution or furcation (Russ, 1990) and suggests that normal membrane restructuring in gal3$^{-/-}$ DCs is impaired. Two contrasting ruffle structures are exemplified in Figure 8Aiv. Comparison of ruffles on cells from different fields among gal3$^{-/-}$ or gal3$^{+/+}$ cell populations revealed no significant difference in these parameter values (data not shown). Thus, gal3$^{-/-}$ cells appear to manifest smaller, less complex membrane structures than gal3$^{+/+}$ cells. Restrictions in normal ruffle formation on gal3$^{-/-}$ cell membranes may be the basis for the reduced cell motility in gal3$^{-/-}$ cells.

DISCUSSION

Our study revealed defective chemotaxis in immature gal3$^{-/-}$ DCs, but upon maturation, gal3$^{-/-}$ DCs appeared to have corrected the *in vitro* migration defect. Impaired migration of immature gal3$^{-/-}$ DCs was also observed *in vivo*. Importantly, we observed attenuated contact hypersensitivity to oxazolone in gal3$^{-/-}$ mice compared to gal3$^{+/+}$ mice in an established model employing a hapten antigen. Because gal3$^{-/-}$ DCs are just as capable in antigen uptake and

processing as gal3$^{+/+}$ cells (Figure 4b), attenuated contact sensitivity observed in gal3$^{-/-}$ mice is probably due to impaired migration of DCs. Our findings suggest that the earliest migration defect present in immature gal3$^{-/-}$ cells may be responsible for the observed decrease in contact dermatitis in gal3$^{-/-}$ animals. Altogether, these results reveal an important role for galectin-3 in DC trafficking. Moreover, we found that immature gal3$^{-/-}$ BMDCs exhibited attenuated signal transduction upon chemokine receptor ligation. In addition, galectin-3 is associated with membrane ruffles and, specifically, lipid rafts in migrating cells, and galectin-3 deficiency results in structural differences in ruffles. Our data suggest that galectin-3 is necessary for the formation of more complex ruffle structures and may also regulate cell migration at least in part by regulating the cell membrane architecture.

Variations in DC migration can be caused by differences in states of cell differentiation and expression levels of adhesion molecules (Cumberbatch *et al.*, 2000). However, we have established that impaired cell migration due to galectin-3 deficiency is not associated with these factors: (1) there are no differences in the levels of cell activation and differentiation markers CD11c, CD205, and 33D1 antigen; major histocompatibility complex class II; and CD86 on gal3$^{-/-}$ and gal3$^{+/+}$ BMiDCs; (2) adhesion and immunomodulatory molecules CD54 (ICAM-1), CD62L (L-selectin), and CD169 (siglec-1) and integrins CD11a (αL), CD18 (β2), CD49c (α3), CD49d (α4), CD51 (αV), and CD61 (β3) are expressed at comparable levels on gal3$^{-/-}$ and gal3$^{+/+}$ BMiDCs; (3) adhesion of gal3$^{-/-}$ and gal3$^{+/+}$ BMiDCs to untreated cell culture plastic and culture plastic treated with collagen type I, fibronectin, and fetal bovine serum is comparable. Moreover, when gal3$^{-/-}$ and gal3$^{+/+}$ BMiDCs are induced to mature in the presence of LPS, surface levels of the above markers are comparably enhanced in both populations. Finally, levels of CC chemokine receptor 5 receptor for MIP1α/CCL3 are similar between gal3$^{-/-}$ and gal3$^{+/+}$ cells (data not shown).

As recombinant galectin-3 has been shown to serve as a chemoattractant for monocytes and macrophages (Sano *et al.*, 2000), galectin-3 secreted by BMiDCs may induce cell migration in a paracrine fashion. By employing a sensitive assay, we have found little to no galectin-3 on cell surfaces of resting DCs. However, we cannot exclude the possibility that galectin-3 is released by cells exposed to chemokine. Nevertheless, our observation of the inability of lactose to inhibit chemotactic migration suggests an intracellular function for galectin-3 in BMiDC, because the chemoattractant activity demonstrated for recombinant galectin-3 is inhibited by lactose (Sano *et al.*, 2000). In addition, the migration defect in gal3$^{-/-}$ BMDCs was noted when engrafted into either gal3$^{-/-}$ or gal3$^{+/+}$ animals (Figure 3a), when engrafted into gal3$^{+/+}$ animals, suggesting that the presence of galectin-3 in the lymphatic environment was unable to correct this defect, (although this difference in the latter) was not statistically significant. These results also point to an intracellular action for galectin-3 in its regulation of cell motility. Furthermore, we present additional data suggesting that galectin-3 may contribute to cell migration by functioning at the cytosolic side apposed to lipid rafts.

Our observed galectin-3 expression in DC appears to diverge from a study of human DCs (Dietz *et al.*, 2000) in that they observed galectin-3 downregulation during culture. We recognize that human monocyte-derived DCs may be dissimilar from mouse bone marrow-derived DCs merely because of species differences. More likely, the differences could be due to cytokine and maturation stimuli used to generate the respective cell lines. Human monocyte-derived DCs were cultured in human serum, GM-CSF, and IL-4 and matured in the presence of IL-6, tumor necrosis factor-α, IL-1β, and prostaglandin E2. The mouse DCs we employed were obtained with GM-CSF in culture with fetal bovine serum and matured by exposure to LPS.

It is noteworthy that the association of galectin-3 in lipid rafts was demonstrated with detergent isolates of mouse macrophages under highly stringent conditions of high pH (Harder and

Simons, 1997) and in the presence of lactose as a lectin inhibitor. These results suggest that this protein does not bind to raft components through lectin–carbohydrate interactions, but likely through protein–protein interactions. In this regard, galectin-3 has been shown to interact with a number of intracellular proteins independent of its lectin properties (Liu *et al.*, 2002), including membraneassociated proteins, such as K-Ras (Elad-Sfadia *et al.*, 2004).

Galectin-3 has been shown to be present in lipid rafts in HeLa cells (Foster *et al.*, 2003) and transformed canine hematopoietic stem cells (Osterhues *et al.*, 2006), although the possibility that galectin-3 is associated with glycoprotein ligands present in raft isolates was not addressed in these studies. Another member of this family, galectin-4, has been identified in highly detergent-resistant superrafts of intestinal microvilli and proposed to function by stabilizing raft assemblies through high-affinity interaction with sulfated raft lipids (Hansen *et al.*, 2001; Ideo *et al.*, 2005). Whether association with lipid rafts is a general property of galectin family members awaits further investigation.

Closely associated with receptor activation by growth factors is rapid formation of membrane ruffles over the cell surface as one of the earliest signs of activation (Bailly *et al.*, 2000). Ruffles reorganize to form migration-associated structures at the leading edge of polarized cells (Honda *et al.*, 1999) and pseudopods (Zigmond and Sullivan, 1979), and this is subsequently followed by activation of signal-propagating molecules (Leblanc *et al.*, 1998). In this regard, we detected atypical distribution of smaller ruffles with lower complexity on $gal3^{-/-}$ cells relative to $gal3^{+/+}$ cells (Figure 8). Lipid rafts have been documented to be involved in motility (Simons and Toomre, 2000; Manes *et al.*, 2001; Pike, 2003; Gomez-Mouton *et al.*, 2004) and are present in close proximity to membrane ruffles (Boyer *et al.*, 2004) and at the leading edges in filopodia and lamellipodia (Manes *et al.*, 2001; Gomez-Mouton *et al.*, 2004). By being positioned at the membrane within actively restructuring ruffle domains, galectin-3 may contribute to stabilization of membrane domains that are critical at the earliest periods of receptor signal transduction (Wiesner *et al.*, 2005).

Our results demonstrating a role for galectin-3 in DC migration suggest that this protein may be important in processes in which DCs are contributory, in particular, innate and adaptive immunity. Our finding that galectin-3 promotes the intensity of contact dermatitis suggests that this protein may be targeted for the treatment of this disease, as well as other inflammatory diseases in which DCs are involved.

MATERIALS AND METHODS

Reagents

rGM-CSF was a generous gift from Kirin Pharmaceuticals (Tokyo, Japan). Fluorescence-tagged antibodies were from Jackson Laboratories (West Grove, PA), Molecular Probes–Invitrogen or Zymed-Invitrogen (Carlsbad, CA). Fluorescence-labeled CTB and phalloidin were from Molecular Probes–Invitrogen. *E. coli* O111:B4 LPS was from List Biologicals (Campbell, CA). Monoclonal anti-vinculin (FVIN-1), collagenase IV, DNase I, FITC, 4-ethoxymethylene-2-phenyl-2-oxazoline-5-one (oxazolone), and Hoechst 33342 were from Sigma (St Louis, MO). $DiOC_{16}$ was purchased from Molecular Probes–Invitrogen. Galectin-3 antibodies were previously described (Frigeri and Liu, 1992; Hsu *et al.*, 1992).

The $gal3^{+/+}$ and $gal3^{-/-}$ mice used were described previously (Hsu *et al.*, 2000) and are congenic in C57BL/6, backcrossed for over nine generations. Mice were matched by age and sex in all assays. All studies were performed according to protocols approved by the Institutional Animal Care and Use Committee and consistent with the National Institutes of Health *Guide for the Care and Use of Laboratory Animals*.

Antibodies used in cell phenotyping were CD11a (M17/4), CD11b (M1/70), CD11c (N418), CD16/CD32 (93), CD18 (M18/2), CD49d (R1-2), CD51 (RMV-7), CD62L (MEL-14), CD80 (16-10A1), CD86 (GL1), 33D1, Gr-1 (RB6-8C5), F4/80 (BM8) from eBioscience (San Diego, CA); CD49a (Ha31/8), CD49c (42), CD54 (3E2), CD61 (2C9 G2), CD169 (E50-2440), CC chemokine receptor 5 (C34-3448) from BD Pharmingen (San Diego, CA); major histocompatibility complex class II (28-16-8S) from Caltag Invitrogen (Carlsbad, CA); and CD205 (NLDC-145) from Serotec (Raleigh, NC). Antibodies to phospho-AKT, AKT, phospho-MAP1/2, MAPK1/2, and MKK4 were obtained from Cell Signaling (Danvers, MA).

Bone marrow cultures

BMiDCs were prepared from bone marrow aspirates according to the described protocols in culture medium containing rGM-CSF at 20 ng ml^{-1} (Inaba *et al.*, 1992; Lutz *et al.*, 1999). Nonadherent cells were transferred to fresh plates after 1 or 2 days in culture, and after an additional 4–5 days in culture, nonadherent cells were gently removed by decanting, leaving in place the regenerating foci. Cells produced from these foci constituted BMiDCs after 10–14 days in culture. Cell surface expression of CD11c by flow cytometry routinely demonstrated over 90% population constituency of this DC marker. BMiDCs were matured by exposure to 2 mg ml^{-1} LPS (*E. coli* O111:B4) for 24 hours.

BMMΦs were prepared as described previously in the presence of rGM-CSF (Sano *et al.*, 2003) and were harvested on day 5 or 6. Over 90% of the cells obtained by this method routinely expressed CD11b and had morphological properties characteristic of monocyte/ macrophages in stained cytospins.

Flow cytometry

Before being stained with antibodies, BMiDCs and BMMΦs were incubated with anti-CD16/32 (Fc-Block) to inactivate Fc receptors according to the manufacturer's instructions. Incubation with antibodies was performed in phosphate-buffered saline with 0.5% (w/v) bovine serum albumin and anti-CD16/32 on ice. Cells were centrifuged and fixed in 1% (w/v) paraformaldehyde before analysis on a Beckman Coulter Epics/XL flow cytometer. Data analysis was performed with FlowJo software (Tree Star, Ashland, OR). Cell surface and total galectin-3 were measured with Alexa488-conjugated polyclonal anti-galectin-3 antibody (Frigeri and Liu, 1992). Fixed J774A.1 macrophage cells were included for each analysis and galectin-3 levels in BMDCs were normalized to levels in J774A.1 for comparative expression analyses.

In vitro chemotaxis

These assays were performed as described (Sano *et al.*, 2000) with mouse chemokines MCP-1/CCL2, MIP-1α/CCL3, and m-CSF (Peprotech, Rocky Hill, NJ) in the lower reservoir. Assay durations were 90 minutes and migrated cells were enumerated after soluble Wright's staining. Five high-power fields were averaged in duplicate or triplicate for each data point.

Subagarose migration assay

Cells were suspended in BMMΦ culture medium and 2.5×10^4 cells were placed into each duplicate or triplicate 3mm well in agarose, prepared as described elsewhere (Grando *et al.*, 1993). Cells were cultured for 10 days with daily medium replacement. Migration was terminated by fixation in 0.25% glutaraldehyde and treated with Wright's stain. Migration distance was determined outwardly from the wall of each 3mm well to edges of migrated cells in triplicate, as described (Chernyavsky *et al.*, 2004).

In vitro adhesion assays

BMiDCs were incubated in 96-well tissue culture plates coated with 50 μg ml^{-1} fibronectin, laminin, collagen type I (Cohesion Technologies, Palo Alto, CA), or 10% fetal bovine serum in phosphate-buffered saline, followed by blocking with 100 μg ml^{-1} BSA as described (Humphries, 1998). $Gal3^{-/-}$ and $gal3^{+/+}$ BMiDCs were incubated in wells for 0.5, 1, and 2 hours, gently washed with phosphate-buffered saline, and fixed in paraformaldehyde. Adherent $gal3^{-/-}$ and $gal3^{+/+}$ cells were compared by measurement of absorbance at 600nm after crystal violet staining (Humphries, 1998).

In vivo migration assays

Wild-type mice were injected with 2×10^6 $gal3^{-/-}$ and $gal3^{+/+}$ BMiDCs labeled with vital dye $DiOC_{16}$ into contralateral hind footpads as described (Del Prete *et al.*, 2004). Popliteal lymph nodes harvested 24 and 48 hours later were treated with collagenase IV and DNase I and processed for flow cytometry.

Cutaneous DC trafficking to lymph nodes was assayed after application of FITC in acetone:dibutyl phthalate (1:1, v/v) to shaved abdomens of mice according to published procedures (Macatonia *et al.*, 1987). DCs from inguinal lymph nodes were obtained following collagenase IV/DNase I digestion. FITC-labeled DCs were analyzed by flow cytometry after staining with phycoerythrinlabeled anti-CD11c, and cell yields were calculated from numbers of FITC-stained cells and cell recoveries for each lymph node.

Cutaneous dendritic cell staining

DCs in epithelial sheets were processed as described (Larsen *et al.*, 1990), obtained by treatment of pinnae with 0.5 M ammonium thiocyanate, acetone fixation, and incubation with anti-class II, followed by FITC-labeled secondary antibody. Images were obtained with a × 20 objective and epithelial DCs were counted from over 40 fields.

Phosphoprotein analyses

BMiDCs were starved in medium containing 0.1% serum for 1 hour and activated with 2.5 μM formyl peptide (fMLP) at 10^7 cells per milliliter at 37°C. Aliquots were removed at 0, 5, 10, and 20 minutes after activation, quenched in cold serum-free medium, and lysed. Protein detection in blots was performed as described (Chen *et al.*, 2006) with phosphoprotein-specific antibodies or for total protein. Ratios of $gal3^{-/-}$ to $gal3^{+/+}$ phosphoprotein were calculated from laser density scans of the film in the following manner: ($gal3^{-/-}$ phosphoprotein/$gal3^{-/-}$ total protein)/($gal3^{+/+}$ phosphoprotein/ $gal3^{+/+}$ total protein).

Contact hypersensitivity

Contact hypersensitivity was induced with oxazalone as described (Wang *et al.*, 1997). Solutions of hapten (3%, w/v) prepared in acetone:olive oil (4:1, v/v) were applied to shaved abdomens of mice. After 5 days, the mice were challenged on one ear with 1% oxazalone (w/v) in acetone:olive oil (4:1, v/v) and solvent only on the other ear. Ear thickness was measured daily for 5 days with a micrometer and swelling was expressed as percentage of ear exposed to hapten over ear treated with solvent. Each group consisted of four or five animals.

Fluorescence microscopy

BMiDCs from 10- to 14-day cultures were adhered and induced on fibronectin-coated coverslips as described (Spangler, 1992). BMiDC adhered to cleaned glass coverslips were activated with 1 μg ml^{-1} fMLP or 10 ng ml^{-1} MCP-1/CCL2 for 20 minutes. Cells were processed for fluorescence microscopy by preblocking with anti-CD16/32, followed by incubation with primary antibody and cross-adsorbed Alexa488- or rhodamine Red-X-tagged

secondary anti-body, as described (Sano *et al.*, 2003). F-actin was visualized with Alexa488-, tetramethylrhodamine-, or Alexa647-conjugated phalloidin, and the nucleus was counterstained with Hoechst 33342. For visualization of lipid rafts, nonpermeabilized cells were incubated with Alexa488- or Alexa555-conjugated CTB (5 μg ml^{-1}) at 12°C as described (Harder *et al.*, 1998), washed, and fixed. Cells were subsequently processed for antibody and phalloidin detection and mounted in FluoromountG (Southern Biotech, Birmingham, AL). Microscopy was performed on an Olympus BX61 with × 60 water objective (NA 1.2), and images were acquired at 0.5 μm intervals with SlideBook 4.1.12 (Intelligent Imaging Innovations, Denver, CO) on a PCO Sensicam CCD camera at full resolution (1,374 × 1,022 pixels). Image deconvolution with the nearest-neighbor algorithm was performed in SlideBook.

Image analyses

Fluorescence micrographs of macrophages or DCs treated in parallel were analyzed according to protocols described by Yi and Coppolino (2006) using ImageJ 1.38u (Rasband, 2007). Co-localization analyses were performed according to the Costes and Manders protocols (Manders *et al.*, 1993; Costes *et al.*, 2004) implemented in public domain ImageJ plug-ins (Collins, 2007). Measurements of ruffles were performed from cultures of BMiDCs induced by adhesion on fibronectin and processed for indirect immunofluorescence staining as described. Ruffles on cells labeled with phalloidin were visualized from projection images of optical sections of entire cells following nearest-neighbor deconvolution. Ruffle edges were demarcated following thresholding of Laplacian of Gaussian filtered projection images (Sonka *et al.*, 1999; Fisher *et al.*, 2004; Yi and Coppolino, 2006; Meijering, 2007), from which shape descriptors for ruffles larger than 11 square pixels, previously determined by inspection to be the smallest area with recognizable ruffle characteristics, were calculated.

Density centrifugation of macrophage cell lysate

The mouse macrophage line J774A.1 was activated with fMLP as described above, lysed in cold Triton X-100, and processed for enrichment of membrane lipid rafts by isopycnic sucrose density (Brown and Rose, 1992; Harder and Simons, 1997; Brown, 1998) ultracentrifugation (Beckman NVT90 rotor). As additional raft concentration by centrifugation was not required, protein concentrations in individual fractions were determined by Bradford assay and immunoblots were performed for detection of galectin-3 and flotillin-1 with anti-galectin-3 and polyclonal anti-flotillin-1 (Santa Cruz Biotechnology, Santa Cruz, CA). Equivalent protein loads were applied to lanes for all experiments.

Statistical analyses

Data were compared by nonparametric statistical analyses by the Mann–Whitney *U*-test/ Wilcoxon two-group test using JMP (SAS Institute, Cary, NC) and determined to be statistically significant for $P \leq 0.05$.

Abbreviations

BMiDC, immature bone marrow-derived dendritic cell
BMMΦ, bone marrow-derived macrophage
CTB, cholera toxin subunit B
DC, dendritic cell
fMLP, formyl peptide MetLeuPhe
ICA, intensity correlation analysis
LPS, lipopolysaccharide
MCP-1, macrophage chemotactic protein-1 (CCL2)
MIP1α, macrophage inflammatory protein-1α (CCL3)

PDM, product difference of the means
rGM-CSF, recombinant granulocyte/macrophage colony-stimulating factor

ACKNOWLEDGMENTS

This study was supported by NIH grants R01 AI20958, R01 AI39620, and P01 AI50498 to F.-T.L. and NIH grant GM62136 and a research grant from the Flight Attendant Medical Research Institute to S.A.G. We thank Dr Akira Takashima and Dr John Apgar for input provided during the preparation of the manuscript, and Dr Carl Ware and Dr Wolfram Ruf for comments on this study. We also thank Dr Suzette Smiley-Jewell for assistance in editing the manuscript.

REFERENCES

Bailly M, Wyckoff J, Bouzahzah B, Hammerman R, Sylvestre V, Cammer M, et al. Epidermal growth factor receptor distribution during chemotactic responses. Mol Biol Cell 2000;11:3873–3883. [PubMed: 11071913]

Banchereau J, Briere F, Caux C, Davoust J, Lebecque S, Liu YJ, et al. Immunobiology of dendritic cells. Annu Rev Immunol 2000;18:767–811. [PubMed: 10837075]

Bickel PE, Scherer PE, Schnitzer JE, Oh P, Lisanti MP, Lodish HF. Flotillin and epidermal surface antigen define a new family of caveolae-associated integral membrane proteins. J Biol Chem 1997;272:13793–13802. [PubMed: 9153235]

Borm B, Requardt RP, Herzog V, Kirfel G. Membrane ruffles in cell migration: indicators of inefficient lamellipodia adhesion and compartments of actin filament reorganization. Exp Cell Res 2005;302:83–95. [PubMed: 15541728]

Boyer L, Travaglione S, Falzano L, Gauthier NC, Popoff MR, Lemichez E, et al. Rac GTPase instructs nuclear factor-kappaB activation by conveying the SCF complex and IkBalpha to the ruffling membranes. Mol Biol Cell 2004;15:1124–1133. [PubMed: 14668491]

Brown DA, Rose JK. Sorting of GPI-anchored proteins to glycolipid-enriched membrane subdomains during transport to the apical cell surface. Cell 1992;68:533–544. [PubMed: 1531449]

Brown RE. Sphingolipid organization in biomembranes: what physical studies of model membranes reveal. J Cell Sci 1998;111(Part 1):1–9. [PubMed: 9394007]

Chen HY, Sharma BB, Yu L, Zuberi R, Weng IC, Kawakami Y, et al. Role of galectin-3 in mast cell functions: galectin-3-deficient mast cells exhibit impaired mediator release and defective JNK expression. J Immunol 2006;177:4991–4997. [PubMed: 17015681]

Chernyavsky AI, Arredondo J, Marubio LM, Grando SA. Differential regulation of keratinocyte chemokinesis and chemotaxis through distinct nicotinic receptor subtypes. J Cell Sci 2004;117:5665–5679. [PubMed: 15494367]

Collins, T. Colocalisation analysis. McMaster Biophotonics Facility ImageJ for Microscopy. 2007. http://www.macbiophotonics.ca/imagej/colour_analysis.htm

Consortium for Functional Glycomics public data. 2008. http://www.functionalglycomics.org/glycomics/publicdata/phenotyping.jsp

Costes SV, Daelemans D, Cho EH, Dobbin Z, Pavlakis G, Lockett S. Automatic and quantitative measurement of protein-protein colocalization in live cells. Biophys J 2004;86:3993–4003. [PubMed: 15189895]

Cumberbatch M, Dearman RJ, Griffiths CE, Kimber I. Langerhans cell migration. Clin Exp Dermatol 2000;25:413–418. [PubMed: 11012599]

Curnock AP, Logan MK, Ward SG. Chemokine signalling: pivoting around multiple phosphoinositide 3-kinases. Immunology 2002;105:125–136. [PubMed: 11872087]

Del Prete A, Vermi W, Dander E, Otero K, Barberis L, Luini W, et al. Defective dendritic cell migration and activation of adaptive immunity in PI3Kgamma-deficient mice. EMBO J 2004;23:3505–3515. [PubMed: 15318168]

Dietz AB, Bulur PA, Knutson GJ, Matasic R, Vuk-Pavlovic S. Maturation of human monocyte-derived dendritic cells studied by microarray hybridization. Biochem Biophys Res Commun 2000;275:731–738. [PubMed: 10973791]

Elad-Sfadia G, Haklai R, Ballan E, Kloog Y. Galectin-3 augments K-Ras activation and triggers a Ras signal that attenuates ERK but not phosphoinositide 3-kinase activity. J Biol Chem 2004;279:34922–34930. [PubMed: 15205467]

Fisher, R.; Perkins, S.; Walker, A.; Wolfart, E. Digital filters. Hypermedia Image Processing Reference 2. 2004. http://homepages.inf.ed.ac.uk/rbf/HIPR2/hipr_top.htm

Forster R, Schubel A, Breitfeld D, Kremmer E, Renner-Muller I, Wolf E, et al. CCR7 coordinates the primary immune response by establishing functional microenvironments in secondary lymphoid organs. Cell 1999;99:23–33. [PubMed: 10520991]

Foster LJ, De Hoog CL, Mann M. Unbiased quantitative proteomics of lipid rafts reveals high specificity for signaling factors. Proc Natl Acad Sci USA 2003;100:5813–5818. [PubMed: 12724530]

Frigeri LG, Liu F-T. Surface expression of functional IgE binding protein, an endogenous lectin, on mast cells and macrophages. J Immunol 1992;148:861–869. [PubMed: 1730878]

Germain RN. An innately interesting decade of research in immunology. Nat Med 2004;10:1307–1320. [PubMed: 15580257]

Gomez-Mouton C, Lacalle RA, Mira E, Jimenez-Baranda S, Barber DF, Carrera AC, et al. Dynamic redistribution of raft domains as an organizing platform for signaling during cell chemotaxis. J Cell Biol 2004;164:759–768. [PubMed: 14981096]

Grando SA, Crosby AM, Zelickson BD, Dahl MV. Agarose gel keratinocyte outgrowth system as a model of skin re-epithelization: requirement of endogenous acetylcholine for outgrowth initiation. J Invest Dermatol 1993;101:804–810. [PubMed: 8245509]

Gungabissoon RA, Bamburg JR. Regulation of growth cone actin dynamics by ADF/cofilin. J Histochem Cytochem 2003;51:411–420. [PubMed: 12642619]

Hansen GH, Immerdal L, Thorsen E, Niels-Christiansen LL, Nystrom BT, Demant EJ, et al. Lipid rafts exist as stable cholesterol-independent microdomains in the brush border membrane of enterocytes. J Biol Chem 2001;276:32338–32344. [PubMed: 11389144]

Harder T, Scheiffele P, Verkade P, Simons K. Lipid domain structure of the plasma membrane revealed by patching of membrane components. J Cell Biol 1998;141:929–942. [PubMed: 9585412]

Harder T, Simons K. Caveolae, DIGs, and the dynamics of sphingolipid-cholesterol microdomains. Curr Opin Cell Biol 1997;9:534–542. [PubMed: 9261060]

Hawkins PT, Anderson KE, Davidson K, Stephens LR. Signalling through Class I PI3Ks in mammalian cells. Biochem Soc Trans 2006;34:647–662. [PubMed: 17052169]

Honda A, Nogami M, Yokozeki T, Yamazaki M, Nakamura H, Watanabe H, et al. Phosphatidylinositol 4-phosphate 5-kinase alpha is a downstream effector of the small G protein ARF6 in membrane ruffle formation. Cell 1999;99:521–532. [PubMed: 10589680]

Hsu DK, Yang R-Y, Yu L, Pan Z, Salomon DR, Fung-Leung W-P, et al. Targeted disruption of the galectin-3 gene results in attenuated peritoneal inflammatory responses. Am J Pathol 2000;156:1073–1083. [PubMed: 10702423]

Hsu DK, Zuberi R, Liu F-T. Biochemical and biophysical characterization of human recombinant IgE-binding protein, an S-type animal lectin. J Biol Chem 1992;267:14167–14174. [PubMed: 1629216]

Hughes RC. Galectins as modulators of cell adhesion. Biochimie 2001;83:667–676. [PubMed: 11522396]

Hume DA. The mononuclear phagocyte system. Curr Opin Immunol 2006;18:49–53. [PubMed: 16338128]

check this page number HumphriesMJCell-Substrate Adhesion Assays1998New York, NYJohn Wiley9.1.1–11

Ideo H, Seko A, Yamashita K. Galectin-4 binds to sulfated glycosphingolipids and carcinoembryonic antigen in patches on the cell surface of human colon adenocarcinoma cells. J Biol Chem 2005;280:4730–4737. [PubMed: 15546874]

Inaba K, Inaba M, Romani N, Aya H, Deguchi M, Ikehara S, et al. Generation of large numbers of dendritic cells from mouse bone marrow cultures supplemented with granulocyte/macrophage colony-stimulating factor. J Exp Med 1992;176:1693. [PubMed: 1460426]

Janeway CAJ, Medzhitov R. Innate immune recognition. Annu Rev Immunol 2002;20:197–216. [PubMed: 11861602]

King CA, Van Heyningen WE. Deactivation of cholera toxin by a sialidase-resistant monosialosylganglioside. J Infect Dis 1973;127:639–647. [PubMed: 4707310]

Larsen CP, Steinman RM, Witmer-Pack M, Hankins DF, Morris PJ, Austyn JM. Migration and maturation of Langerhans cells in skin transplants and explants. J Exp Med 1990;172:1483–1493. [PubMed: 2230654]

Leblanc V, Tocque B, Delumeau I. Ras-GAP controls Rho-mediated cytoskeletal reorganization through its SH3 domain. Mol Cell Biol 1998;18:5567–5578. [PubMed: 9710640]

Li Q, Lau A, Morris TJ, Guo L, Fordyce CB, Stanley EF. A syntaxin 1, Galpha(o), and N-type calcium channel complex at a presynaptic nerve terminal: analysis by quantitative immunocolocalization. J Neurosci 2004;24:4070–4081. [PubMed: 15102922]

Liu FT. Regulatory roles of galectins in the immune response. Int Arch Allergy Immunol 2005;136:385–400. [PubMed: 15775687]

Liu FT, Patterson RJ, Wang JL. Intracellular functions of galectins. Biochim Biophys Acta 2002;1572:263–273. [PubMed: 12223274]

Lutz MB, Kukutsch N, Ogilvie AL, Rossner S, Koch F, Romani N, et al. An advanced culture method for generating large quantities of highly pure dendritic cells from mouse bone marrow. J Immunol Methods 1999;223:77–92. [PubMed: 10037236]

Ma Y, Pope RM. The role of macrophages in rheumatoid arthritis. Curr Pharm Des 2005;11:569–580. [PubMed: 15720276]

Macatonia SE, Knight SC, Edwards AJ, Griffiths S, Fryer P. Localization of antigen on lymph node dendritic cells after exposure to the contact sensitizer fluorescein isothiocyanate. Functional and morphological studies. J Exp Med 1987;166:1654–1667. [PubMed: 3119761]

Manders EM, Verbeek FJ, Aten JA. Measurement of co-localization of objects in dual-colour confocal images. J Microsc 1993;169:375–382.

Manes S, Lacalle RA, Gomez-Mouton C, del Real G, Mira E, Martinez-A C. Membrane raft microdomains in chemokine receptor function. Semin Immunol 2001;13:147–157. [PubMed: 11308298]

Meijering, E. FeatureJ, A Java Package for Image Feature Extraction. 2007. http://www.imagescience.org/meijering/software/featurej/index.html

Nakahara S, Oka N, Raz A. On the role of galectin-3 in cancer apoptosis. Apoptosis 2005;10:267–275. [PubMed: 15843888]

Osterhues A, Liebmann S, Schmid M, Buk D, Huss R, Graeve L, et al. Stem cells and experimental leukemia can be distinguished by lipid raft protein composition. Stem Cells Dev 2006;15:677–686. [PubMed: 17105403]

Palucka KA, Taquet N, Sanchez-Chapuis F, Gluckman JC. Dendritic cells as the terminal stage of monocyte differentiation. J Immunol 1998;160:4587–4595. [PubMed: 9574566]

Parton RG, Simons K. Digging into caveolae. Science 1995;269:1398–1399. [PubMed: 7660120]

Piemonti L, Bernasconi S, Luini W, Trobonjaca Z, Minty A, Allavena P, et al. IL-13 supports differentiation of dendritic cells from circulating precursors in concert with GM-CSF. Eur Cytokine Netw 1995;6:245–252. [PubMed: 8789290]

Pike LJ. Lipid rafts: bringing order to chaos. J Lipid Res 2003;44:655–667. [PubMed: 12562849]

Rasband, W. ImageJ, Image Processing and Analysis in Java. 2007. http://rsb.info.nih.gov/ij/

Ridley AJ, Schwartz MA, Burridge K, Firtel RA, Ginsberg MH, Borisy G, et al. Cell migration: integrating signals from front to back. Science 2003;302:1704–1709. [PubMed: 14657486]

Russ, JC. Computer Assisted Microscopy. New York: Plenum Press; 1990. Image measurements; p. 175-218.

Sallusto F, Lanzavecchia A. Efficient presentation of soluble antigen by cultured human dendritic cells is maintained by granulocyte/macrophage colony-stimulating factor plus interleukin 4 and downregulated by tumor necrosis factor alpha. J Exp Med 1994;179:1109–1118. [PubMed: 8145033]

Sano H, Hsu DK, Apgar JR, Yu L, Sharma BB, Kuwabara I, et al. Critical role of galectin-3 in phagocytosis by macrophages. J Clin Invest 2003;112:389–397. [PubMed: 12897206]

Sano H, Hsu DK, Yu L, Apgar JR, Kuwabara I, Yamanaka T, et al. Human galectin-3 is a novel chemoattractant for monocytes and macrophages. J Immunol 2000;165:2156–2164. [PubMed: 10925302]

Schluger NW, Rom WN. Early responses to infection: chemokines as mediators of inflammation. Curr Opin Immunol 1997;9:504–508. [PubMed: 9287176]

Simons K, Toomre D. Lipid rafts and signal transduction. Nat Rev Mol Cell Biol 2000;1:31–39. [PubMed: 11413487]

Smart EJ, Ying YS, Mineo C, Anderson RG. A detergent-free method for purifying caveolae membrane from tissue culture cells. Proc Natl Acad Sci USA 1995;92:10104–10108. [PubMed: 7479734]

Sonka, M.; Hlavac, V.; Boyle, R. Image Processing, Analysis, and Machine Vision. PWS Publishing: Pacific Grove; 1999. Image pre-processing; p. 57-118.

Spangler BD. Structure and function of cholera toxin and the related *Escherichia coli* heat-labile enterotoxin. Microbiol Rev 1992;56:622–647. [PubMed: 1480112]

Thomas R, MacDonald KP, Pettit AR, Cavanagh LL, Padmanabha J, Zehntner S. Dendritic cells and the pathogenesis of rheumatoid arthritis. J Leukoc Biol 1999;66:286–292. [PubMed: 10449169]

Wang B, Fujisawa H, Zhuang L, Kondo S, Shivji GM, Kim CS, et al. Depressed Langerhans cell migration and reduced contact hypersensitivity response in mice lacking TNF receptor p75. J Immunol 1997;159:6148–6155. [PubMed: 9550416]

Wiesner S, Legate KR, Fassler R. Integrin-actin interactions. Cell Mol Life Sci 2005;62:1081–1099. [PubMed: 15761669]

Yi Q, Coppolino MG. Automated classification and quantification of F-actin-containing ruffles in confocal micrographs. Biotechniques 2006;40:745–750. [PubMed: 16774118]

Zigmond SH, Sullivan SJ. Sensory adaptation of leukocytes to chemotactic peptides. J Cell Biol 1979;82:517–527. [PubMed: 479314]

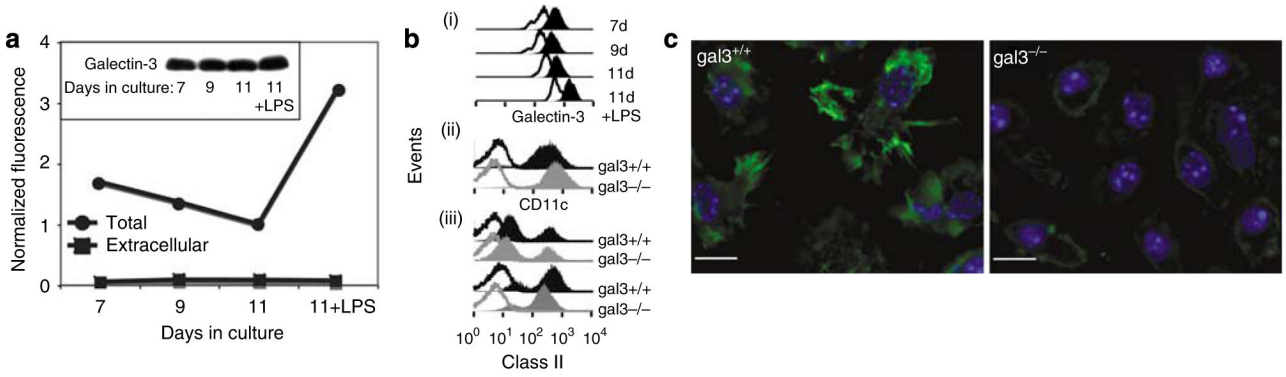

Figure 1. Galectin-3 is expressed in bone marrow-derived dendritic cells

Immature DCs were prepared from bone marrow cultures in the presence of rGM-CSF, and mature DCs were obtained by additional treatment of immature DCs with *E. coli* lipopolysaccharide. (**a**) Galectin-3 levels measured by flow cytometry. BMiDCs or LPS-matured DCs were treated with Fc-Block and directly processed with anti-galectin-3 antibody for detection of cell surface galectin-3, or fixed, permeabilized, and incubated with the antibody in the presence of Fc-Block for detection of intracellular galectin-3. Mean fluorescence intensities were obtained after corrections for nonspecific primary antibody and normalized to levels of galectin-3 relative to J774A.1, obtained concurrently at each time point. Inset, galectin-3 levels determined by immunoblotting from equivalent cell loads of BMiDCs and mature DCs as above. (**b**) Flow cytometry for detection of intracellular galectin-3, CD11c, and class II. (i) Galectin-3, (ii) CD11c, and (iii) class II on BMDCs summarized in (**a**). Unshaded histogram, antibody control; shaded histogram, galectin-3 antibody. (**c**) Galectin-3 detected by indirect immunofluorescence microscopy. $Gal3^{-/-}$ and $gal3^{+/+}$ BMiDCs were activated with MCP-1 and processed for visualization of galectin-3 with polyclonal anti-galectin-3 after fixation and permeabilization. Nuclear staining with Hoechst 33342 is also shown. Images were obtained with an Olympus IX61 with × 60 objective (NA 1.2). Bar represents a distance of 10 μm.

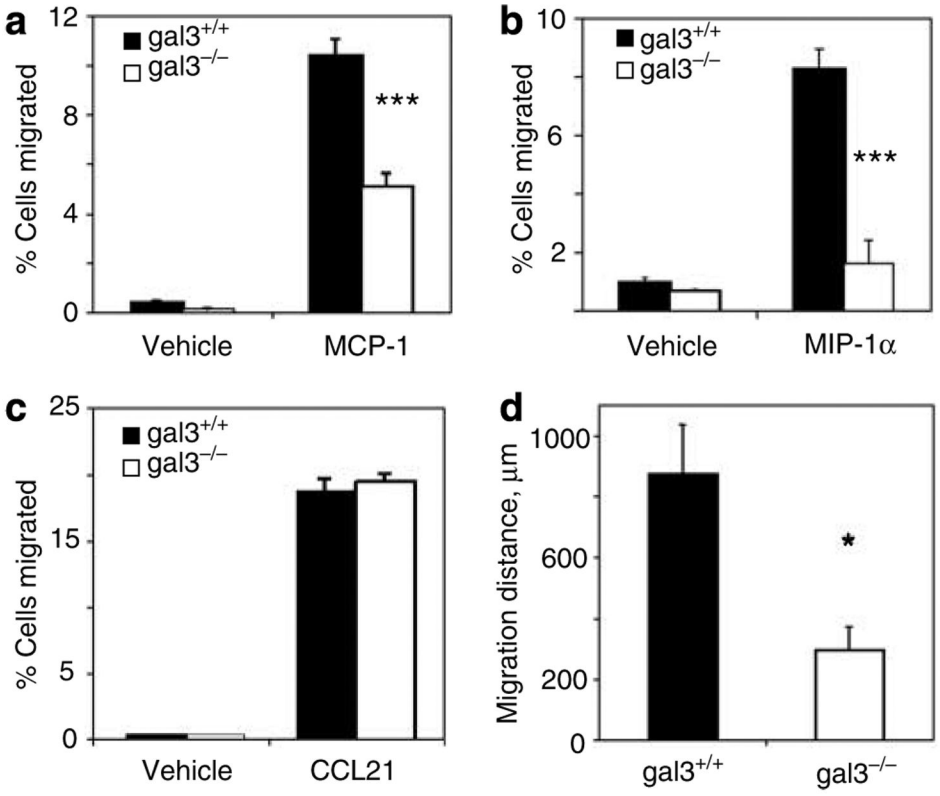

Figure 2. Defective *in vitro* migration of galectin-3-deficient bone marrow-derived immature dendritic cells and macrophages

Chemotaxis of BMiDCs from gal3$^{-/-}$ and gal3$^{+/+}$mice to MCP-1/CCL2 (**a**) and MIP1α/CCL3 (**b**) was assessed in micro Boyden chambers. Each well contained 3×10^4 cells, and assays were performed in triplicate. (**c**) Chemotaxis of BMDCs, matured in 2 μg ml^{-1} LPS for 24 hours as above, to CCL21. (**d**) Nonchemotactic migration of gal3$^{-/-}$ and gal3$^{+/+}$ BMMΦ in an agarose invasion assay. Results are means ± SE from one representative experiment of three. **P*<0.05; ****P*<0.001.

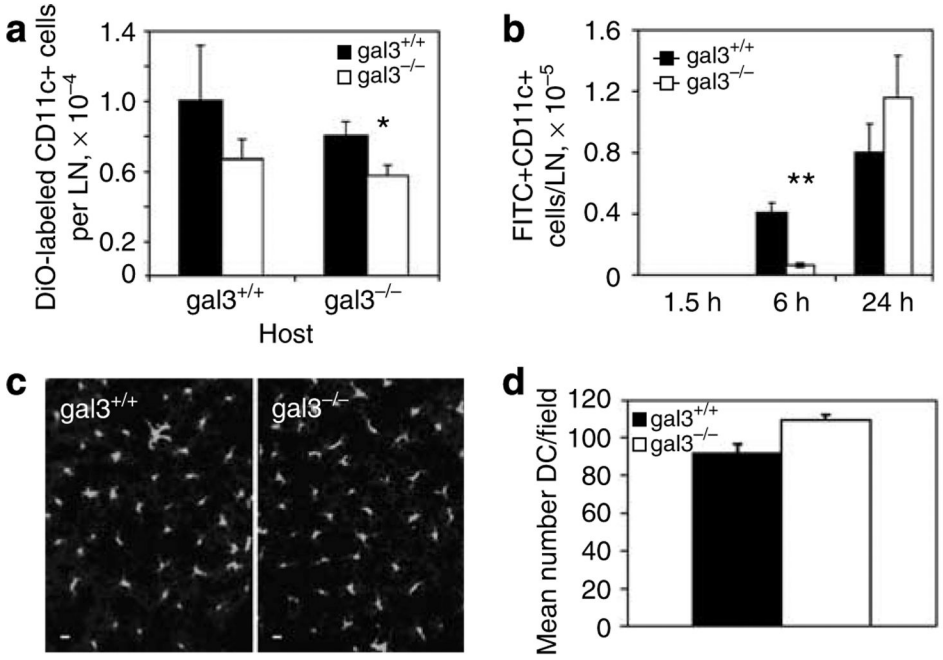

Figure 3. Impaired *in vivo* migration of bone marrow-derived immature dendritic cells from galectin-3-deficient mice

(**a**) $DiOC_{16}$-labeled BMiDCs (2×10^6) from $gal3^{-/-}$ and $gal3^{+/+}$ mice were injected into contralateral footpads of $gal3^{+/+}$ and $gal3^{-/-}$ mice. Fluorescent $CD11c^+$ DCs in inguinal lymph nodes were counted by flow cytometry 2 days later. Data are means ± SE from one of three experiments. **P*<0.05. (**b**) Fluorescein isothiocyanate was applied to the lower abdomens of $gal3^{-/-}$ and $gal3^{+/+}$ mice, and $CD11c^+$ lymph node cells from digested inguinal nodes were analyzed by flow cytometry at the indicated periods. At time 0, cells were isolated immediately after fluorescein application. Data are means ± SE from a representative experiment of two. Four to six mice per genotype were used in each experiment. ***P*<0.01. (**c**) Major histocompatibility complex class II^+ cells in epidermis from $gal3^{-/-}$ and $gal3^{+/+}$ mouse pinnae were visualized by epifluorescence microscopy on an Olympus IX61 with a × 20 objective (NA 0.7). Bars represent a distance of 10 μm. Contrasts were adjusted identically to improve visibility. (**d**) Numbers of epidermal DCs from five contiguous micrograph fields (original magnification × 20) are shown for $gal3^{-/-}$ and $gal3^{+/+}$ mice, means ± SE.

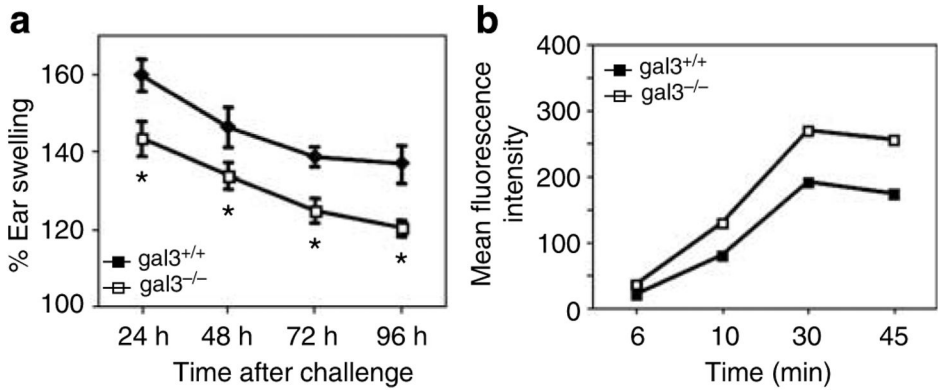

Figure 4. Galectin-3-deficient mice exhibit reduced contact hypersensitivity but possess normal antigen-processing capabilities

(**a**) Mice were treated on the abdomen with oxazalone and challenged 5 days later on one ear with the hapten and on the contralateral ear with solvent. Ear swelling was determined by measurements with a micrometer. Each experiment was performed with 4 or 5 mice per genotype, and data are means ± SE of two combined experiments. **P*<0.05. (**b**) Uptake and processing of poorly fluorescent DQ-OVA in immature BMiDCs followed by flow-cytometric measurements of fluorescence at the indicated times. Data are representative of two experiments.

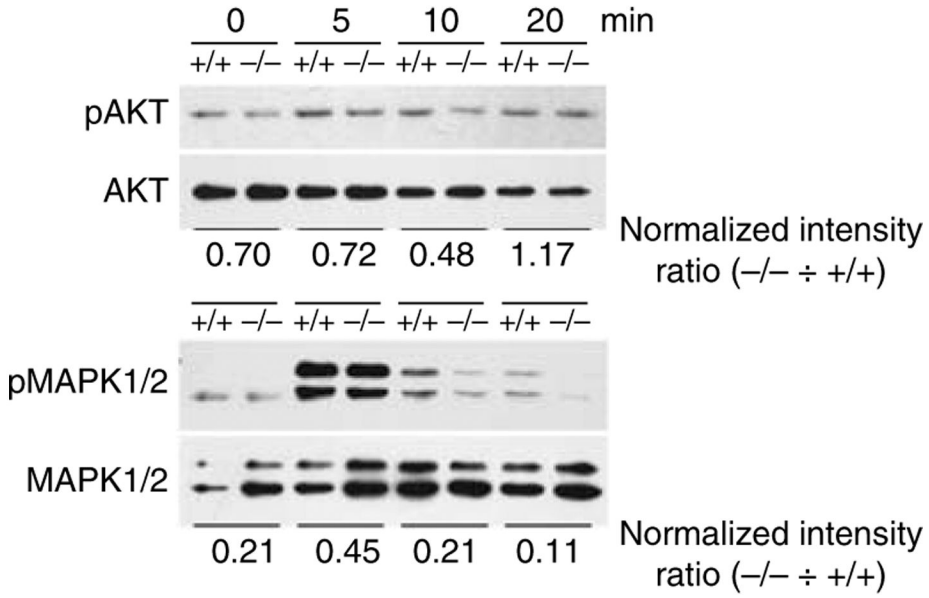

Figure 5. Immature gal3$^{-/-}$ DCs exhibit signaling defects in response to chemokine

Gal3$^{+/+}$ and gal3$^{-/-}$ BMiDCs were activated with 2.5 μM fMLP and equivalent cell numbers were harvested at the indicated periods. Cell lysates were processed for immunoblotting analysis to detect phosphorylated proteins and total protein. Numbers underneath each panel represent ratios of normalized phosphoprotein levels in gal3$^{-/-}$ cells divided by the corresponding levels in gal3$^{+/+}$ cells.

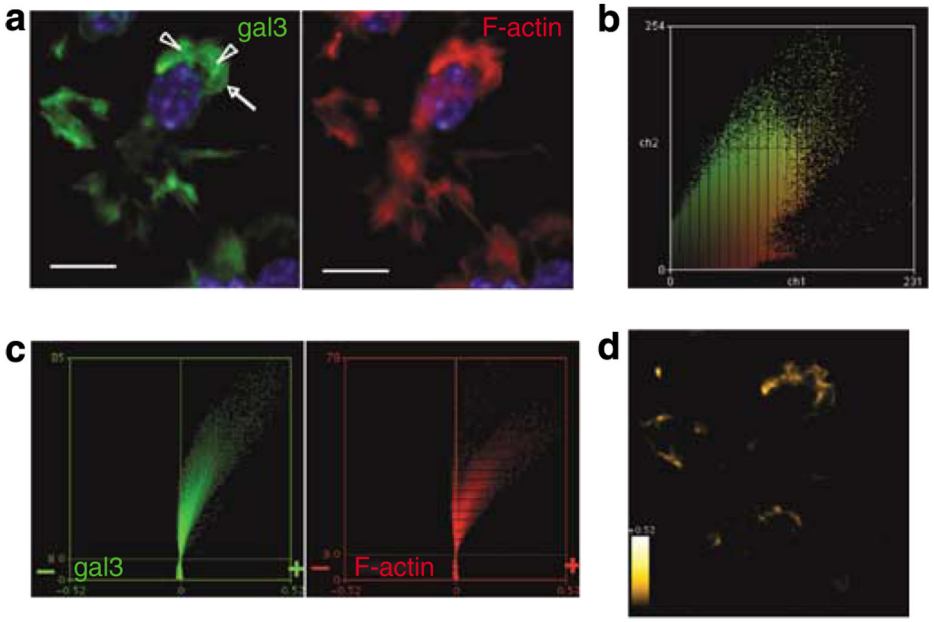

Figure 6. Galectin-3 is localized in membrane ruffles of immature bone marrow-derived dendritic cells

BMiDC motility was induced by adhesion on fibronectin-coated coverslips and exposure to fMLP. (**a**) Detection of intracellular galectin-3 with antibody in the presence of Fc-Block, and F-actin with labeled phalloidin in the projection image. Fluorescence micrographs were acquired in permeabilized cells with a × 60 objective (NA 1.2) at intervals of 0.5 μm and deconvolved from optical planes of the entire cell. Images are contrast enhanced to improve visibility. Arrowheads and arrows indicate ruffles and lamellipodia, respectively. The bar represents a distance of 10 mm. (**b**) Diagonal distribution of galectin-3 (green) and F-actin (red) staining of all optical planes from unenhanced images of the field depicted in (**a**) indicates co-dependent pixel intensities. (**c**) Intensity correlation analyses of thresholded unenhanced images show pronounced positive skewing of PDM (product difference of the means, see Materials and Methods) values for galectin-3 and F-actin, indicative of significant co-localization. (**d**) Regions of the cell demonstrating galectin-3 and F-actin co-localization from positive PDM guidance in (**c**) are shown. Heat scale, PDM values 0 to ±0.52. Image is contrast enhanced to improve visibility. Results are representative of two experiments.

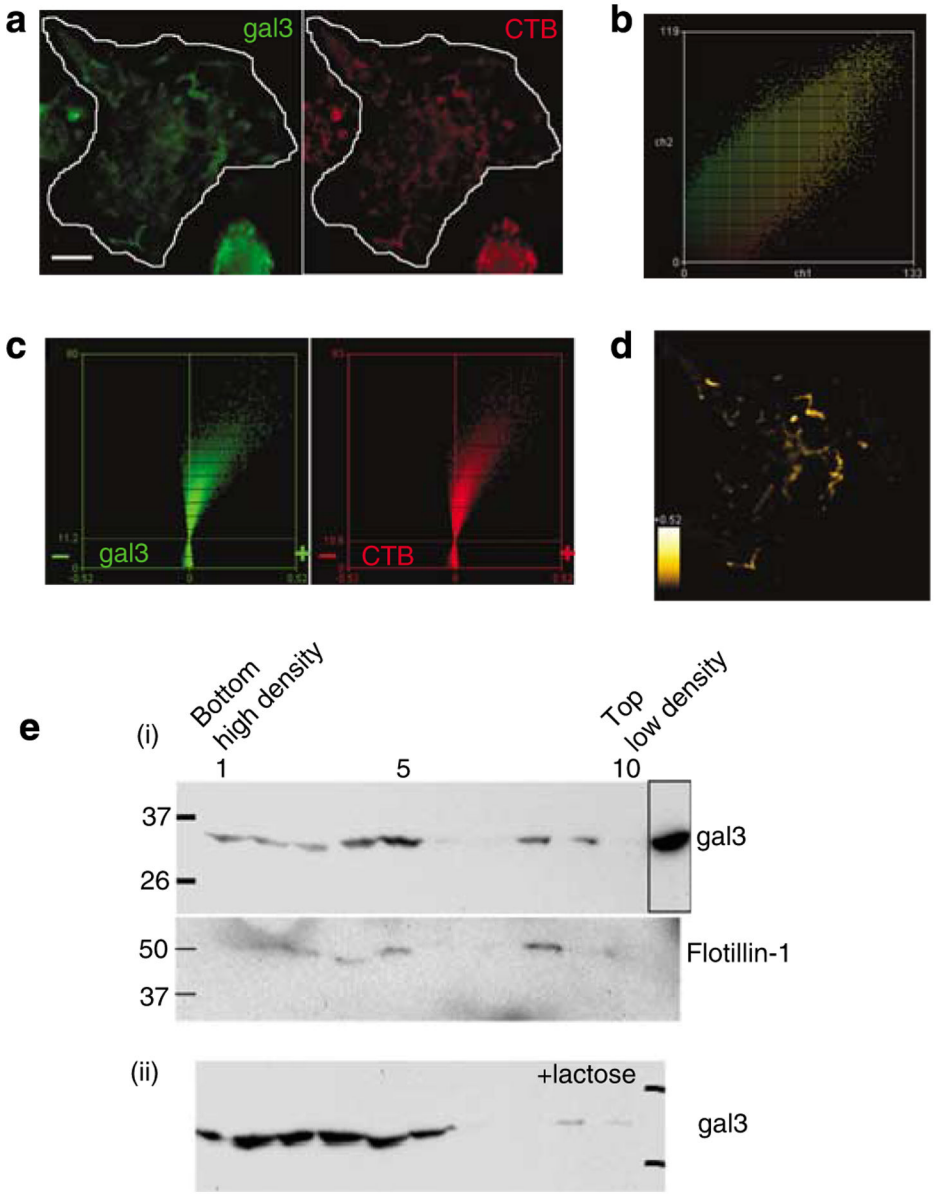

Figure 7. Galectin-3 is present in lipid rafts of mouse dendritic cells

BMiDCs were induced with fibronectin and fMLP as in Figure 6. (**a**) Cells were incubated with Alexa555-labeled CTB at 12 °C, followed by fixation, permeabilization, and development for fluorescence detection of intracellular galectin-3 as in Figure 6. Micrographs were acquired with a × 60 objective (NA 1.2) at intervals of 0.5 μm and deconvolved as described. Projection images shown are contrast enhanced to improve visualization. The bar represents a distance of 10 μm. (**b**) Diagonal distribution of galectin-3 (green) and CTB (red) staining of all optical planes from unenhanced images of the field depicted in (**a**) indicates co-dependent pixel intensities. (**c**) Intensity correlation analyses of thresholded unenhanced images show pronounced positive skewing of PDM (product difference of the means; see Materials and Methods) values for galectin-3 and CTB, indicative of significant co-localization. (**d**) Regions of the cell demonstrating galectin-3 and CTB co-localization from positive PDM guidance in (**c**) are shown. Heat scale, PDM values 0 to +0.52. Image is contrast enhanced to improve

visibility. Results are representative of two experiments. (**e**) Immunoblots for galectin-3 from fMLP-activated J774A.1 macrophages homogenized in cold Triton X-100 buffer and fractionated on sucrose gradients. Equal protein loads from each fraction were processed for detection of specific proteins (i) galectin-3, absence of lactose, and the lipid raft marker flotillin-1; and (ii) galectin-3, presence of 100m$_M$ lactose in the sucrose gradient. High- to low-density fractions appear from left to right, and the boxed region represents unfractionated cell lysate. Size markers in kilodaltons are shown. These results are representative of three experiments.

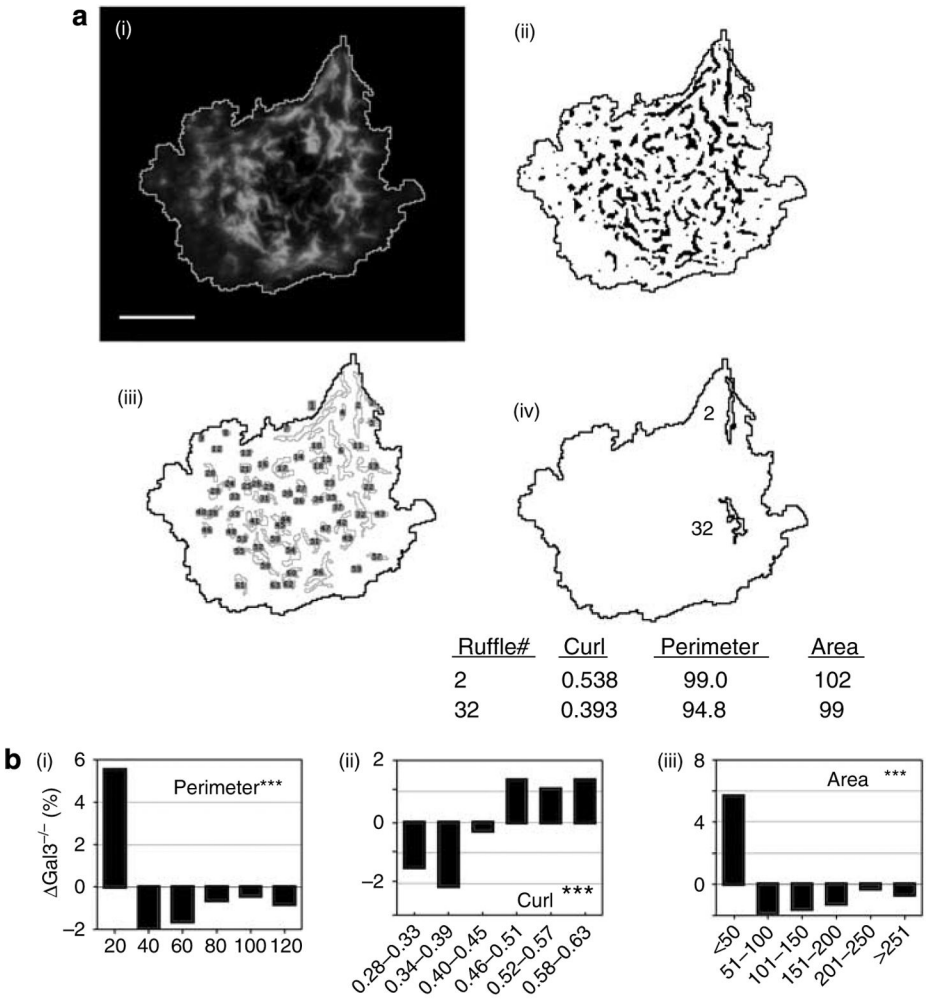

Figure 8. Membrane ruffles of gal3$^{-/-}$ bone marrow-derived cells differ from those of gal3$^{+/+}$ cells

(**a**) A projection image obtained from deconvolved micrographs of cells from BMiDC cultures stained with tetramethylrhodamine-labeled phalloidin (i) induced to migrate on fibronectin-coated coverslips for 20 minutes. Cell outlines were established after thresholding (see Materials and Methods), and surface ruffles were demarcated after Laplacian of Gaussian filtering and thresholding (see Materials and Methods) in ImageJ. The bar represents a distance of 5 μm. (ii) Ruffles greater than 11 square pixels were identified (iii) and physical measurements were obtained (see Materials and Methods). The image in the lower right (iv) shows two ruffles of approximately equal areas with higher (2) and lower (32) curl values, representing extended and convoluted structures, respectively, that exemplify 63 ruffles in this cell visualized after processing by ImageJ. (**b**) Shape descriptors determined from migrating cells (see Materials and Methods) show divergent distributions in gal3$^{-/-}$ versus gal3$^{+/+}$ ruffle populations for (i) perimeter, (ii) curl, and (iii) area. For each parameter, bars represent the change in the population of gal3$^{-/-}$ ruffles of the parameter shown on the *x* axis, relative to gal3$^{+/+}$. Over 1,500 gal3$^{-/-}$ and gal3$^{+/+}$ individual ruffle measurements were obtained from a total of over 20 cells from five contiguous high-power fields for each genotype. Dimensions are arbitrary pixel units, representative of two experiments. ***P 0.001 for each parameter comparison.